

Infrared Spectra of Aluminum Hydrides in Solid Hydrogen: Al₂H₄ and Al₂H₆

Xuefeng Wang,[§] Lester Andrews,^{*,§} Simon Tam,^{||,†} Michelle E. DeRose,^{||} and
Mario E. Fajardo^{||,‡}

Contribution from the Department of Chemistry, P.O. Box 400319, University of Virginia,
Charlottesville, Virginia 22904-4319, U.S. Air Force Research Laboratory, AFRL/PRSP,
Edwards AFB, California 93524-7680

Received March 28, 2003; E-mail: isa@virginia.edu

Abstract: The reaction of laser-ablated Al atoms and normal-H₂ during co-deposition at 3.5 K produces AlH, AlH₂, and AlH₃ based on infrared spectra and the results of isotopic substitution (D₂, H₂ + D₂ mixtures, HD). Four new bands are assigned to Al₂H₄ from annealing, photochemistry, and agreement with frequencies calculated using density functional theory. Ultraviolet photolysis markedly increases the yield of AlH₃ and seven new absorptions for Al₂H₆ in the infrared spectrum of the solid hydrogen sample. These frequencies include terminal Al–H₂ and bridge Al–H–Al stretching and AlH₂ bending modes, which are accurately predicted by quantum chemical calculations for dibridged Al₂H₆, a molecule isostructural with diborane. Annealing these samples to remove the H₂ matrix decreases the sharp AlH₃ and Al₂H₆ absorptions and forms broad 1720 ± 20 and 720 ± 20 cm⁻¹ bands, which are due to solid (AlH₃)_n. Complementary experiments with thermal Al atoms and para-H₂ at 2.4 K give similar spectra and most product frequencies within 2 cm⁻¹. Although many volatile binary boron hydride compounds are known, binary aluminum hydride chemistry is limited to the polymeric (AlH₃)_n solid. Our experimental characterization of the dibridged Al₂H₆ molecule provides an important link between the chemistries of boron and aluminum.

Introduction

Boron hydride chemistry has been investigated for a century, and a large number of distinct boron hydride compounds have been identified and characterized;^{1–4} however, aluminum hydride chemistry under normal conditions is limited to the nonvolatile polymeric solid trihydride (AlH₃)_n.^{4–6} The diborane molecule is fundamentally important, and the textbook example of hydrogen (μ -hydrido) bridge bonding.⁴ Although the isostructural dialane molecule is calculated to be stable by several groups,^{7–13} molecular Al₂H₆ has not been isolated even though

the binding energy for dialane is calculated to be only slightly smaller than that for diborane but significantly larger than computed for digallane.^{8,10} The failure to observe dialane is even more surprising in view of the recent synthesis of digallane, which yielded an isostructural Ga₂H₆ molecule.^{14–16} However, the properties of solid gallane suggest a discrete oligomer, such as (GaH₃)₄, which retains terminal M–H bonds,¹⁶ unlike solid (AlH₃)_n, which contains only Al–H–Al bridge bonds.⁵ The only experimental evidence for Al₂H₆ is mass spectrometric detection of trace Al₂H₆⁺ cation^{17–19} and a broad photodetachment spectrum of Al₂H₆[–] anion.²⁰ Surface science investigations suggest that aluminum hydrides such as AlH, AlH₃, and Al₂H₆ desorb at elevated temperatures from Al metal surfaces containing (AlH₃)_n or adsorbed hydrogen.^{18–22}

Since the dimerization of AlH₃ is exothermic by about 35 kcal/mol depending on the theoretical methods employed,^{8,10,11,20} the direct Al₂H₆ preparation involves the dimerization of AlH₃. Alane (AlH₃) has been observed by three groups from reactions

* To whom correspondence should be addressed.

§ University of Virginia.

|| U.S. Air Force Research Laboratory.

† Present Address: KLA-Tencor Corp., 1 Technology Drive, Milpitas, CA 95035.

‡ Present Address: U.S. Air Force Research Laboratory, AFRL/MNME, Eglin AFB, FL 32542.

- (1) Stock, A. *Hydrides of Boron and Silicon*; Cornell University Press: Ithaca, 1933.
- (2) Lipscomb, W. N. *Boron Hydrides*; W. A. Benjamin: New York, 1963.
- (3) Greenwood, N. N. *Chem. Soc. Rev.* **1992**, 21, 49.
- (4) Cotton, F. A.; Wilkinson, G.; Murillo, C. A.; Bochmann, M. *Advanced Inorganic Chemistry*, 6th ed.; Wiley: New York, 1999.
- (5) Turley, J. W.; Rinn, H. W. *Inorg. Chem.* **1969**, 8, 18.
- (6) Brower, F. M.; Matzek, N. E.; Reigler, P. F.; Rinn, H. W.; Roberts, C. B.; Schmidt, D. L.; Snover, J. A.; Terada, K. *J. Am. Chem. Soc.* **1976**, 98, 2450.
- (7) Liang, C.; Davy, R. D.; Schaeffer, H. F., III. *Chem. Phys. Lett.* **1989**, 159, 393.
- (8) Lammertsma, K.; Leszczynski, J. *J. Phys. Chem.* **1990**, 94, 2806.
- (9) Bock, C. W.; Trachtman, M.; Murphy, C.; Muschert, B.; Mains, G. J. *J. Phys. Chem.* **1991**, 95, 2339.
- (10) Duke, B. J.; Liang, C.; Schaeffer, H. F., III. *J. Am. Chem. Soc.* **1991**, 113, 2884.
- (11) Shen, M.; Schaefer, H. F., III. *J. Chem. Phys.* **1992**, 96, 2868.
- (12) Barone, V.; Orlandini, L.; Adamo, C. *J. Phys. Chem.* **1994**, 98, 13185.
- (13) Magers, D. H.; Hood, R. B.; Leszczynski, J. *Int. J. Quantum Chem. Symp.* **1994**, 28, 579.
- (14) Downs, A. J.; Goode, M. J.; Pulham, C. R. *J. Am. Chem. Soc.* **1989**, 111, 1936.
- (15) Pulham, C. R.; Downs, A. J.; Goode, M. J.; Rankin, D. W. H.; Robertson, H. E. *J. Am. Chem. Soc.* **1991**, 113, 5149.
- (16) Downs, A. J.; Pulham, C. R. *Chem. Soc. Rev.* **1994**, 1994, 175.
- (17) Siegel, B. *J. Am. Chem. Soc.* **1960**, 82, 1535.
- (18) Breisacher, P.; Siegel, B. *J. Am. Chem. Soc.* **1964**, 86, 5053.
- (19) Hara, M.; Domen, K.; Onishi, T.; Nozoye, H. *J. Phys. Chem.* **1991**, 95, 6.
- (20) Rao, B. K.; Jena, P.; Burkart, S.; Ganteför, G.; Seifert, G. *Phys. Rev. Lett.* **2001**, 86, 692.
- (21) Kohdoh, H.; Hara, M.; Domen, K.; Nozoye, H. *Surf. Sci.* **1993**, 287–288, 74.
- (22) Zhu, Y. F.; Shehadeh, R.; Grant, E. R. *J. Chem. Phys.* **1992**, 97, 883.

of energetic aluminum atoms with hydrogen in solid argon and characterized by infrared spectroscopy;^{23–26} however, the concentration of AlH_3 was not sufficient to form Al_2H_6 in the rigid argon matrix. Our successful synthesis of Al_2H_6 for the first time involves pure hydrogen as the matrix.^{27–29} This ensures the selective formation of the highest monohydride AlH_3 , and diffusion on annealing the soft hydrogen matrix to 6.5 K allows dimerization to Al_2H_6 . Similar laser ablation experiments with boron and hydrogen give B_2H_6 .^{30,31} A preliminary account of this work has been reported.³²

Experimental and Theoretical Methods

The experiments for reaction of laser-ablated aluminum atoms with hydrogen during condensation in excess argon and neon have been described previously.^{23,30,33,34} The Nd:YAG laser fundamental (1064 nm, 10 Hz repetition rate with 10 ns pulse width) was focused (10 cm f.l. lens) onto a rotating aluminum target (Johnson Matthey, 99.998%). The laser energy was varied from 10 to 20 mJ/pulse at the sample. Laser-ablated aluminum atoms were co-deposited with 60 STPcc of pure normal hydrogen or deuterium (Matheson) or 120 STPcc of Ne/H_2 or Ne/D_2 onto a 3.5 K CsI cryogenic window for 25–30 min or for 50–60 min. Mixed isotopic HD (Cambridge Isotopic Laboratories), and $\text{H}_2 + \text{D}_2$ samples were used in different experiments. FTIR spectra were recorded at 0.5 cm^{-1} resolution on Nicolet 750 with 0.1 cm^{-1} accuracy using an MCTB detector. Matrix samples were annealed at different temperatures using resistance heat, and selected samples were subjected to filtered broadband photolysis by a medium-pressure mercury arc lamp (Philips, 175W) with globe removed for 20 min periods.

Complementary thermal Al experiments in para- H_2 were performed at Edwards AFB. Samples were prepared by co-deposition of Al atoms from a commercial thermal effusive source (EPI SUMO) and a fast flow of precooled para- H_2 gas³⁵ onto a BaF_2 substrate cooled to $T \approx 2$ K in a liquid helium bath cryostat.³⁶ Operation of the ortho/para converter at $T = 15$ K yields ≈ 100 ppm residual ortho- H_2 content. Infrared absorbance spectra were recorded with a Bruker IFS120HR spectrometer at resolutions of 0.02–0.1 cm^{-1} ; sample thickness and dopant concentrations are calculated from these spectra as described previously.^{31,37} Ultraviolet absorption spectra (not shown) were recorded during some sample depositions, resulting in very weak irradiation and the consequent appearance of minor photolysis products in the deposited samples. Samples were deliberately photolyzed in the ultraviolet using an unfiltered 30 W deuterium lamp located ~ 8 cm from the deposition substrate.

Density functional theory (DFT) calculations of aluminum hydride frequencies are given for comparison with experimental values. The Gaussian 98 program³⁸ was employed with the 6-311++G** basis set for hydrogen and aluminum.³⁹ All geometrical parameters were fully optimized with the B3LYP and BPW91 density functionals,^{40–44} and analytical vibrational frequencies were obtained at the optimized structures.

- (23) Chertihin, G. V.; Andrews, L. *J. Phys. Chem.* **1993**, *97*, 10295.
- (24) Kurth, F. A.; Eberlein, R. A.; Schnöckel, H.; Downs, A. J.; Pulham, C. R. *J. Chem. Soc., Chem. Commun.* **1993**, 1302.
- (25) Pullumbi, P.; Mijoule, C.; Manceron, L.; Bouteiller, Y. *Chem. Phys.* **1994**, *185*, 13.
- (26) Pullumbi, P.; Bouteiller, Y.; Manceron, L.; Mijoule, C. *Chem. Phys.* **1994**, *185*, 25.
- (27) Weltner, W., Jr.; Van Zee, R. J.; Li, S. *J. Phys. Chem.* **1995**, *99*, 6277.
- (28) Fajardo, M. E.; Tam, S.; Thompson, T. L.; Cordonnier, M. E. *Chem. Phys.* **1994**, *189*, 351.
- (29) Wang, X.; Andrews, L. *J. Phys. Chem. A* **2003**, *107*, 570.
- (30) Andrews, L.; Wang, X. *J. Am. Chem. Soc.* **2002**, *124*, 7280.
- (31) Tam, S.; MacIer, M.; DeRose, M. E.; Fajardo, M. E. *J. Chem. Phys.* **2000**, *113*, 9067.
- (32) Andrews, L.; Wang, X. *Science* **2003**, *299*, 2049.
- (33) Andrews, L.; Burkholder, T. R.; Yustein, J. T. *J. Phys. Chem.* **1992**, *96*, 10182.
- (34) Andrews, L.; Citra, A. *Chem. Rev.* **2002**, *102*, 885.
- (35) Tam, S.; Fajardo, M. *Rev. Sci. Instr.* **1999**, *70*, 1926.
- (36) Fajardo, M. E.; Tam, S. *J. Chem. Phys.* **1998**, *108*, 4237.
- (37) Tam, S.; Fajardo, M. E. *Appl. Spectrosc.* **2001**, *55*, 1634.

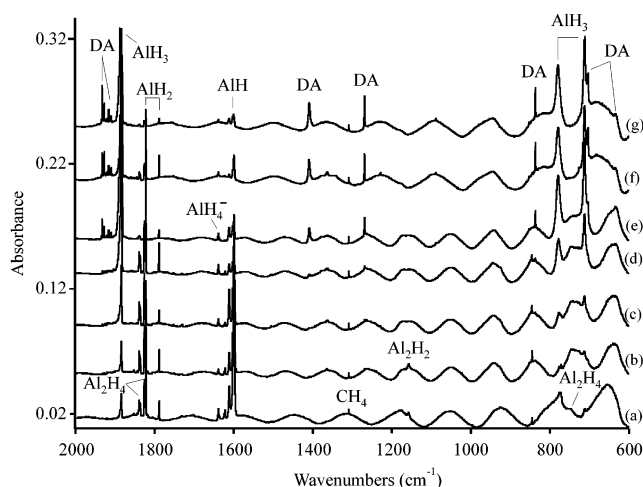


Figure 1. Infrared spectra in the 2000–1100 and 900–600 cm^{-1} regions for laser-ablated Al co-deposited with normal hydrogen at 3.5 K: (a) spectrum of sample deposited for 25 min, (b) after annealing to 6.2 K, (c) after $\lambda > 380$ nm photolysis, (d) after $\lambda > 290$ nm photolysis, (e) after $\lambda > 240$ nm photolysis, (f) after annealing to 6.5 K, and (g) after second $\lambda > 240$ nm photolysis.

Results

Laser-ablated Al atoms were co-deposited with pure normal hydrogen, neon/ H_2 , and argon/ H_2 samples; thermal Al atoms were reacted with para- H_2 ; and new infrared absorptions will be presented along with supporting density functional calculations of aluminum hydrides.

Hydrogen. Aluminum atoms were co-deposited with normal hydrogen using three different laser energies and different sample irradiations: spectra from the lowest laser energy investigation are illustrated in Figure 1. The spectrum of the deposited sample is dominated by the strong AlH absorption at 1598.7 cm^{-1} , which is intermediate between the gas phase (1624.4 cm^{-1})^{45,46} and argon matrix (1590.7 cm^{-1}) absorptions^{23–25,47} for diatomic AlH . A weak 3141.4 cm^{-1} band (1% of 1598.7 cm^{-1} absorbance) appears to be the overtone. The ω_{ex} value deduced for AlH in solid hydrogen, 28.0 cm^{-1} , is slightly smaller than the gas-phase value, 29.1 cm^{-1} , and the ω_{e} value for AlH in solid hydrogen, 1654.7 cm^{-1} , is 27.9 cm^{-1} lower than the gas-phase value.

- (38) Frisch, M. J.; Trucks, G. W.; Schlegel, H. B.; Scuseria, G. E.; Robb, M. A.; Cheeseman, J. R.; Zakrzewski, V. G.; Montgomery, J. A., Jr.; Stratmann, R. E.; Burant, J. C.; Dapprich, S.; Millam, J. M.; Daniels, A. D.; Kudin, K. N.; Strain, M. C.; Farkas, O.; Tomasi, J.; Barone, V.; Cossi, M.; Cammi, R.; Mennucci, B.; Pomelli, C.; Adamo, C.; Clifford, S.; Ochterski, J.; Petersson, G. A.; Ayala, P. Y.; Cui, Q.; Morokuma, K.; Malick, D. K.; Rabuck, A. D.; Raghavachari, K.; Foresman, J. B.; Cioslowski, J.; Ortiz, J. V.; Stefanov, B. B.; Liu, G.; Liashenko, A.; Piskorz, P.; Komaromi, I.; Gomperts, R.; Martin, R. L.; Fox, D. J.; Keith, T.; Al-Laham, M. A.; Peng, C. Y.; Nanayakkara, A.; Gonzalez, C.; Challacombe, M.; Gill, P. M. W.; Johnson, B.; Chen, W.; Wong, M. W.; Andres, J. L.; Gonzalez, C.; Head-Gordon, M.; Replogle, E. S.; Pople, J. A. *Gaussian 98, Revision A.6*; Gaussian, Inc.: Pittsburgh, PA, 1998.
- (39) (a) Krishnan, R.; Binkley, J. S.; Seeger, R.; Pople, J. A. *J. Chem. Phys.* **1980**, *72*, 650. (b) Frisch, M. J.; Pople, J. A.; Binkley, J. S. *J. Chem. Phys.* **1984**, *80*, 3265.
- (40) Becke, A. D. *Phys. Rev. A* **1988**, *38*, 3098.
- (41) Perdew, J. P.; Wang, Y. *Phys. Rev. B* **1992**, *45*, 13244.
- (42) Becke, A. D. *J. Chem. Phys.* **1993**, *98*, 5648.
- (43) Lee, C.; Yang, E.; Parr, R. G. *Phys. Rev. B* **1988**, *37*, 785.
- (44) Stevens, P. J.; Devlin, F. J.; Chablowski, C. F.; Frisch, M. J. *J. Phys. Chem.* **1994**, *98*, 11623.
- (45) Huber, K. P.; Herzberg, G. *Constants of Diatomic Molecules*; Van Nostrand: Princeton, 1979.
- (46) Deutsch, J. L.; Neil, W. S.; Ramsay, D. A. *J. Mol. Spectrosc.* **1987**, *125*, 115.
- (47) Wright, R. B.; Bates, J. K.; Gruen, D. M. *Inorg. Chem.* **1978**, *17*, 2275.

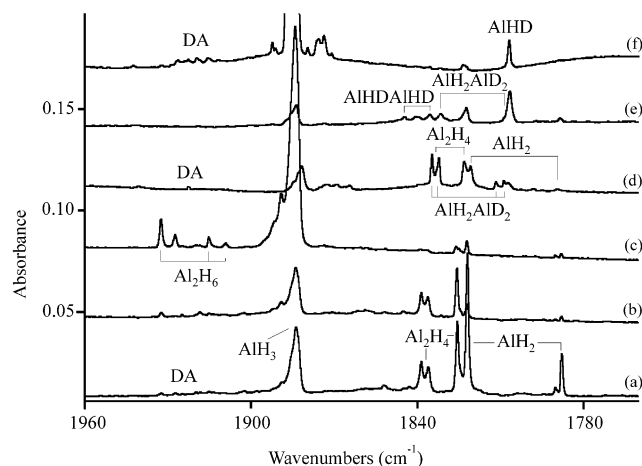


Figure 2. Infrared spectra in the 1960–1760 cm^{-1} region for laser-ablated Al co-deposited with isotopic hydrogen samples at 3.5 K: (a) pure H_2 and Al deposited, (b) after $\lambda > 380$ nm photolysis, (c) after $\lambda > 240$ nm photolysis, (d) 35% H_2 + 65% D_2 and Al deposited, (e) pure HD and Al deposited, and (f) after annealing to 7.3 K.

Absorptions are also observed for AlH_3 (1883.7, 777.9, 711.3 cm^{-1}) and AlH_2 (1821.9, 1787.8 cm^{-1}), which are approximately 1, -5, 14 cm^{-1} and 16, 18 cm^{-1} higher than argon matrix values.^{23–26} New absorptions are observed at 1838.4, 1835.8, 1825.5, 747 cm^{-1} (labeled Al_2H_4), at 1638.1 cm^{-1} (labeled AlH_4^-),⁴⁸ at 1156.1 cm^{-1} (labeled Al_2H_2)²³ with the hint of very weak absorptions at 1932.3, 1915.1, 1408.1, 1268.2, 835.6, 702.4, 631.9 cm^{-1} (labeled DA) (Figure 1a). Annealing to 6.2 K increased all bands except AlH and AlH_4^- (Figure 1b). Photolysis stepwise at $\lambda > 380$, 290, 240 nm destroyed the Al_2H_2 absorption, decreased the AlH band, and increased the AlH_3 absorptions 2 \times , 6 \times , and 13 \times and the DA band set 2 \times , 4 \times , and 16 \times (Figure 1c,d,e). A subsequent annealing to 6.5 K increased all but the 1638 cm^{-1} band (Figure 1f), and a final $\lambda > 240$ nm irradiation increased the DA bands another 25% (Figure 1g). These experiments were remarkably free of oxide impurities: Al_2O was typically $A < 0.001$ at 995.2 cm^{-1} on deposition,³³ and HO_2 was not detected.⁴⁹

Similar behavior was found in the other hydrogen experiments. Although irradiation at $\lambda > 630$ nm had no discernible effect, $\lambda > 530$ nm photolysis destroyed the 1156.1 cm^{-1} band, slightly decreased AlH_2 bands, slightly increased Al_2H_4 and DA bands, and left the sharp 844.1 cm^{-1} band unchanged. Irradiation at $\lambda > 380$ nm slightly decreased Al_2H_4 peaks and markedly decreased AlH_2 , whereas $\lambda > 240$ nm virtually destroyed Al_2H_4 with significant increases in AlH_3 and DA absorptions (Figure 2). Another spectrum after $\lambda > 240$ nm photolysis is shown in Figure 3a including the solid hydrogen absorptions at 4220 and 4149 cm^{-1} . Annealing to 6.8 K allows H_2 to evaporate: solid H_2 absorptions, AlH_3 bands, and DA absorptions decrease by 80–90%, and broad absorptions appear at 1720 ± 20 and 720 ± 20 cm^{-1} (Figure 3b). Further annealing to 7.0 K allows all H_2 to evaporate, all sharp absorptions disappear, and the broad absorptions remain (Figure 3c). These broad bands decrease steadily on annealing to room temperature where 50% of the broad absorbance remains.

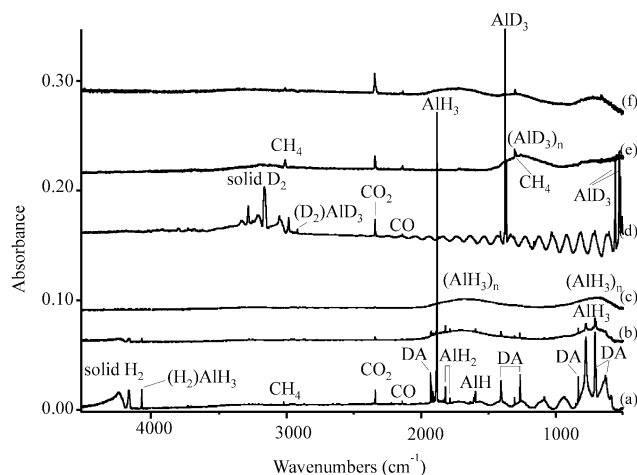


Figure 3. Infrared spectra in the 4500–500 cm^{-1} region for laser-ablated Al co-deposited with isotopic hydrogen samples at 3.5 K: (a) pure H_2 and Al deposited and subjected to $\lambda > 240$ nm photolysis, (b) after annealing to 6.8 K, (c) after annealing to 7.0 K, (d) pure D_2 and Al deposited and subjected to $\lambda > 240$ nm photolysis, (e) after annealing to 14 K, (f) 40% H_2 + 60% D_2 and Al deposited, photolyzed $\lambda > 240$ nm, and annealed to 13 K.

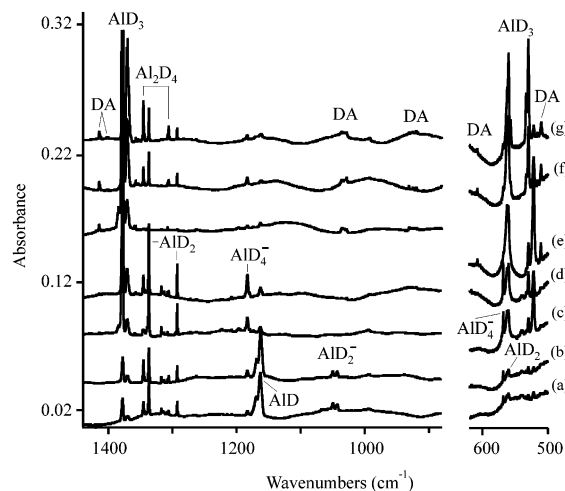


Figure 4. Infrared spectra in the 1440–880 and 620–500 cm^{-1} regions for laser-ablated Al co-deposited with normal deuterium at 3.5 K: (a) spectrum of sample deposited for 25 min, (f) after annealing to 7.3 K, (c) after $\lambda > 290$ nm photolysis, (d) after annealing to 7.5 K, (e) after $\lambda > 240$ nm photolysis, (f) after annealing to 8.0 K, and (g) after annealing to 9.0 K.

Al atoms and D_2 were co-deposited in three experiments, and spectra from the sample prepared using higher laser energy are shown in Figure 4. The AID_x product absorptions observed on deposition include AID_3 , Al_2D_4 , AID_2 , AID , and Al_2D_2 as listed in Table 1. The DA peaks appear on $\lambda > 290$ nm photolysis, increase markedly on $\lambda > 240$ nm irradiation, and increase slightly on subsequent 8.0 K annealing (Figure 4c,e,f). One difference: new bands at 1050.0 and 1043.0 cm^{-1} with D_2 have no H_2 counterparts. On $\lambda > 290$ nm photolysis, these bands give way to the 1183.2 cm^{-1} counterpart (AID_4^-) of the 1638.1 cm^{-1} absorption in solid hydrogen. Further annealing to 9.0 K increases Al_2D_4 bands 2-fold with a small decrease in AID_2 absorptions (Figure 4g). Note that solid D_2 can be annealed about 3 K warmer than solid H_2 before the solid evaporates. Annealing to 9.3 K reveals decreased sharp product absorptions, annealing to 10.2 K markedly decreases solid D_2 bands at 3286, 3168, 2982 cm^{-1} , and the new product bands, and produces a

(48) Pullumbi, P.; Bouteiller, Y.; Manceron, L. *J. Chem. Phys.* **1994**, *101*, 3610.

(49) (a) Wang, X.; Andrews, L.; Chertihin, G. V.; Souter, P. F. *J. Phys. Chem. A* **2002**, *106*, 6302. (b) Wang, X.; Andrews, L. *J. Am. Chem. Soc.* **2003**, *125*, 6581.

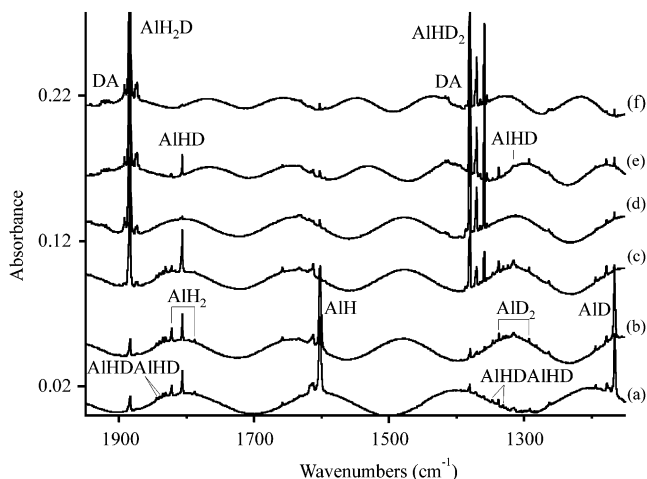
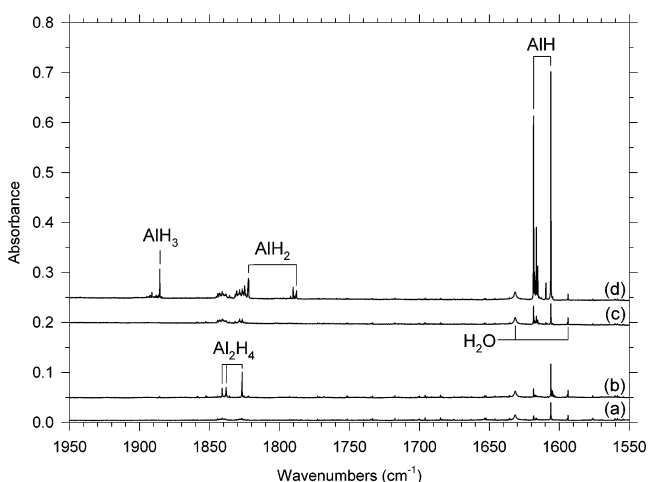
Table 1. Infrared Absorptions (cm^{-1}) Observed from Codeposition of Laser-Ablated Al Atoms and with Ne/H_2 , Pure Normal H_2 , and Ar/H_2 at 3.5 K

Ne/H_2	Ne/D_2	H_2	D_2	Ar/H_2	identification
		4061.6	2919.6		$(\text{H}_2)\text{AlH}_3$
		3141.4			AlH (2ν)
1931.4	1415.8	1932.3	1414.9	1922.2	DA
		1927.2	1413.4	1911.4	DA site
1923.1	1396.1	1915.1	1402.9	1905.7	DA
		1909.1	1401.0	1897.3	DA site
1889.1	1381.3	1883.7	1378.7	1882.6	AlH_3 (ν_3 , e)
		1851.8			Al_xH_y
1840.8	1345.8	1838.4	1346.1	1822.8	Al_2H_4
		1835.8			Al_2H_4
		1825.5	1306.4	1812.0	Al_2H_4
1828.6	1340.4	1821.9	1337.2	1806.0	AlH_2 (ν_3 , b_2)
1794.7	1296.0	1787.8	1293.1	1769.6	AlH_2 (ν_1 , a_1)
		1751.2	1272.4	1743.7	
1627.8	1186.9	1638.1	1183.2	1608.8	AlH_4^-
		1610.7	1169.6		AlH site
1610.8	1171.0	1598.7	1163.1	1590.7	AlH
		1504.9			AlH_4^-
			1050.0		AlD_2^-
			1043.0		AlD_2^-
1404.7	1032.5	1408.1	1028.5	1388.0	DA
1260.2	925.3	1268.2	919.7	1243.4	DA
		1156.1	852.0		Al_2H_2
		924	696		$\text{HAl(H)}_3\text{Al}$
		844.1			$\text{HAl(H)}_3\text{Al}$
835.0	607.3	835.6	607.5		DA
782.9	562.9	777.9	561.8	783.5	AlH_3 (ν_4 , e)
770.7		770.5	568.2	766	AlH_4^-
		770.5	560.3	766	AlH_2
		747	563		Al_2H_4
712.2	523.2	711.3	522.0	697.7	AlH_3 (ν_2 , a_2'')
703.1	511.6	702.4	510.6		DA
630.2		631.9			DA

broad $1260 \pm 20 \text{ cm}^{-1}$ absorption. Further annealing to 14 K removes D_2 and leaves the broad band with weak CH_4 , CO , and CO_2 peaks (Figure 3e). At about 50 K, CH_4 and CO evaporate, but the broad $1260 \pm 20 \text{ cm}^{-1}$ band and CO_2 remain. This broad band decreases about 50% on warming to room temperature.

Three experiments were done with different $\text{H}_2 + \text{D}_2$ mixtures, and both Al–H and Al–D regions reveal strong bands in the spectrum of a 35% $\text{H}_2 + 65\%$ D_2 sample; detail from the Al–H region is shown in Figure 2d. Slight shifts in peaks are due to the change from pure H_2 , but several new absorptions arise from isotopic mixing. As the matrix host evaporates at 9–10 K, the sharp product absorptions decrease, and broad bands appear, and on annealing to 13 K the broad bands remain at 1740 ± 20 , 1280 ± 20 , and 710 ± 20 on the salt window (Figure 3f). One experiment was performed with pure HD, and the 1950–1150 cm^{-1} region is illustrated in Figure 5. More detail is shown in Figure 2e,f, where four new, sharp bands were observed near 1920 cm^{-1} .

Thermal aluminum atoms were co-deposited with para- H_2 at 2.4 K using Al concentrations ranging from 7 to 100 ppm. Spectra from the most dilute sample are shown in Figure 6 where the product bands are weak: AlH is dominant at 1606.0 cm^{-1} . Warming to 4.8 K increased weak 1840.9, 1838.3, 1826.8 cm^{-1} (Al_2H_4) and 1155.0 cm^{-1} (not shown) (Al_2H_2) bands, and ultraviolet photolysis for 10 min produced new 1885.5, 1825.0, 1822.0, 1790.2, and 1787.9 cm^{-1} absorptions (labeled AlH_3 and AlH_2), markedly increased AlH (1618.4, 1606.0 cm^{-1}), and destroyed the 1155.0 cm^{-1} band. All of these absorption features show complicated reversible temperature

**Figure 5.** Infrared spectra in the 1950–1150 cm^{-1} range for laser-ablated Al co-deposited with pure HD at 3.5 K: (a) spectrum of sample deposited for 25 min, (b) after annealing to 6.8 K, (c) after $\lambda > 290 \text{ nm}$ photolysis, (d) after $\lambda > 240 \text{ nm}$ photolysis, (e) after annealing to 7.3 K, and (f) after $\lambda > 240 \text{ nm}$ photolysis.**Figure 6.** Infrared spectra in the 1950–1550 cm^{-1} region of a 1.45-mm-thick para- H_2 sample doped with 7 ppm Al atoms from a thermal effusive source at $T = 950 \text{ }^\circ\text{C}$; sample deposition time = 120 min: (a) deposited sample at $T = 2.4 \text{ K}$, (b) obtained during annealing at $T = 4.8 \text{ K}$ for about 60 min, (c) annealed sample cooled back to $T = 2.5 \text{ K}$, and (d) effects of irradiation with an unfiltered deuterium lamp for 10 min. Spectral resolution is 0.1 cm^{-1} .

dependences, possibly due to the reversible formation of ortho- H_2 /dopant clusters; however, this hypothesis is still under investigation. Of significance here is the fact that the main absorption features in solid para- H_2 appear within $\pm 2 \text{ cm}^{-1}$ of the corresponding absorptions in a normal- H_2 host.

A similar experiment with 100 ppm Al produced stronger Al_2H_2 and Al_2H_4 bands on deposition (Figure 7a). A longer ultraviolet photolysis produced strong AlH_3 and AlH bands and weak DA bands at 1933.5, 1918.6, 1406.1, 1264.3 (Figure 7b), and 835.2 cm^{-1} (the BaF_2 substrate reduces the reliability of spectra below 800 cm^{-1}). Annealing to 4.8 K for 60 min slightly increased the product absorptions (Figure 7c). Finally, high-resolution spectra are shown in the 1950–1750 cm^{-1} region in Figure 8. Since this thinner sample was deposited in only 30 min, it received much less ultraviolet exposure. Thus much weaker bands are observed on sample deposition at 2.4 K (Figure 8a), but growth of the AlH_3 , AlH_2 , and AlH bands is obvious on photolysis (Figure 8b). Of most interest is the “clean”

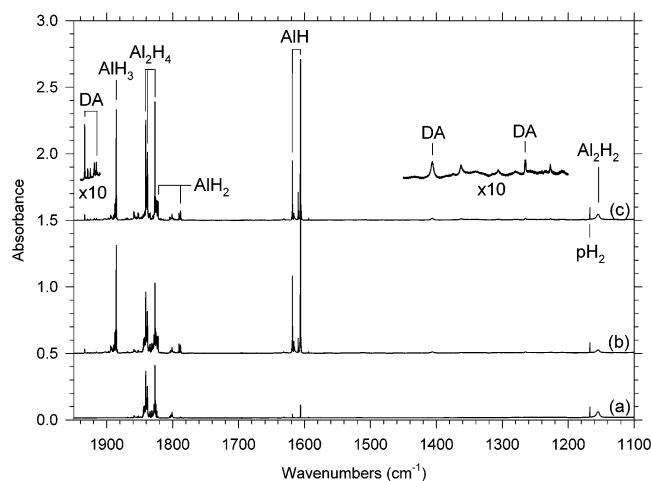


Figure 7. Infrared spectra in the 1950–1100 cm^{-1} region of a 1.48-mm-thick para- H_2 sample doped with 100 ppm Al atoms from a thermal effusive source at $T = 1075\text{ }^\circ\text{C}$; sample deposition time = 120 min: (a) deposited sample at $T = 2.4\text{ K}$, (b) obtained at $T = 2.4\text{ K}$ after irradiation with an unfiltered deuterium lamp for 30 min, and (c) sample cooled back to $T = 2.4\text{ K}$ after annealing at $T = 4.8\text{ K}$ for 60 min. Spectral resolution is 0.05 cm^{-1} .

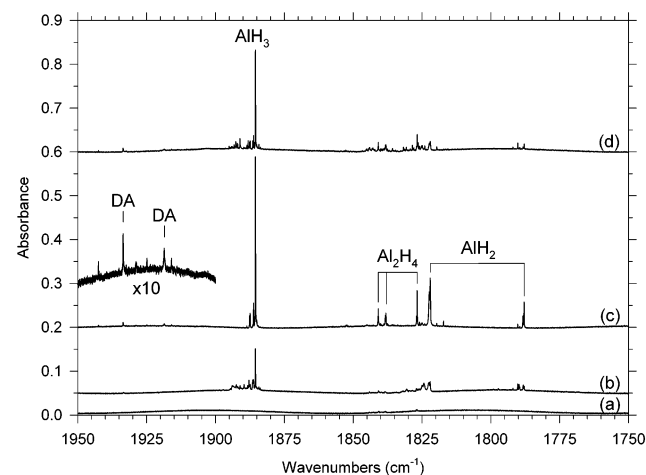


Figure 8. Infrared spectra in the 1950–1750 cm^{-1} region of a 0.40-mm-thick para- H_2 sample doped with 20 ppm Al atoms from a thermal effusive source at $T = 1000\text{ }^\circ\text{C}$; sample deposition time = 30 min: (a) deposited sample at $T = 2.4\text{ K}$, (b) obtained at $T = 2.4\text{ K}$ after irradiation with an unfiltered deuterium lamp for 30 min, (c) obtained during annealing to $T = 4.6\text{ K}$ for 60 min, and (d) sample cooled back to $T = 2.4\text{ K}$. Spectral resolution is 0.02 cm^{-1} .

spectrum recorded during annealing at 4.6 K (Figure 8c), which reveals a sharp dominant 1885.5 cm^{-1} AlH_3 absorption, sharp Al_2H_4 bands at 1840.9 , 1838.3 , and 1826.8 cm^{-1} , sharp AlH_2 bands at 1822.0 , 1787.9 cm^{-1} , and DA bands at 1933.6 , 1918.6 cm^{-1} . A sharp Al_2H_4 band is also observed at 747.8 cm^{-1} .

Neon. Neon matrix investigations were performed with high hydrogen concentrations to favor higher hydrides. Figure 9 illustrates spectra from a 10% H_2 in neon experiment. The strong absorptions in the first spectrum at 1889.1 and 1828.6 cm^{-1} (Figure 9a) are immediately recognized as AlH_3 and AlH_2 from their blue shifts relative to hydrogen and argon matrix absorptions for these molecules. Weak absorptions at 1931.4 , 1923.1 , 1404.7 , and 1260.2 cm^{-1} (labeled DA) in the first spectrum increase on photolysis and annealing (Figure 9b–d). The deuterium counterparts from a similar 10% D_2 experiment are listed in Table 1.

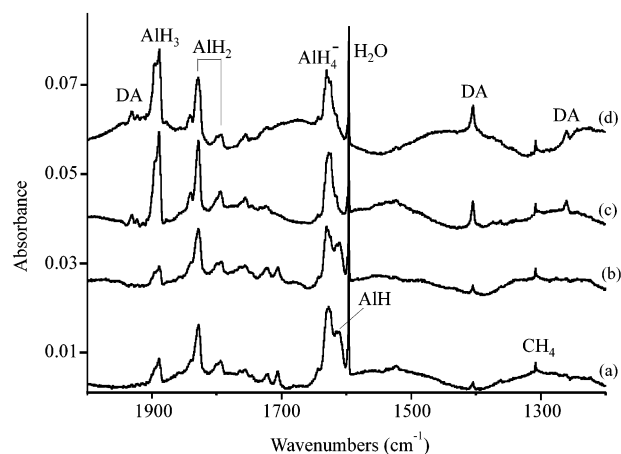


Figure 9. Infrared spectra in the 2000–1200 cm^{-1} range for laser-ablated Al co-deposited with neon + 10% H_2 at 3.5 K: (a) spectrum of sample deposited for 50 min, (b) after annealing to 7.0 K, (c) after $\lambda > 240\text{ nm}$ photolysis, and (d) after annealing to 7.6 K.

Argon. Argon matrix experiments were done with 10% H_2 to compare with the present neon and earlier argon/dilute H_2 work.²³ Product absorptions in the deposited spectrum (Table 1) are in agreement with previous assignments to AlH , AlH_2 , AlH_3 , and AlH_4^- in solid argon.^{23–26,47,48} Neither HO_2 nor AlO_2 absorptions were detected, but a weak Al_2O band was observed at 992.4 cm^{-1} .^{32,49} Satellite absorptions at 1811.8 and 1777.3 cm^{-1} are appropriate for the $(\text{H}_2)\text{AlH}_2$ complex.^{23,25} Annealing to 10–12 K had little effect on the spectrum. Irradiation at $\lambda > 290\text{ nm}$ decreased AlH_2 and AlH bands but increased AlH_3 and AlH_4^- absorptions. Subsequent annealing to 16 K increased absorptions at 1822.8 and 1812.0 cm^{-1} and produced weak new bands at 1922.2 , 1388.0 , and 1243.4 cm^{-1} . Subsequent $\lambda > 240\text{ nm}$ irradiation and 23 K annealing continued these trends.

Calculations. Density functional calculations were performed at the B3LYP/6-311++G** level to provide a consistent set of frequencies for aluminum hydrides and their partially and fully deuterated counterparts to assist in the identification of the new Al_2H_4 and Al_2H_6 molecules observed here. We recomputed Al_2H_2 for comparison.^{23,50} Our results are presented in Tables 2 and 3. The frequencies and bond lengths calculated for AlH_2 , AlH_3 , and AlH_4^- are in line with previous work.^{23–26,48} We also find AlH_2^- to be a stable anion with lower frequencies than AlH_4^- .

Our B3LYP calculations reach the same conclusions about Al_2H_4 isomers as the previous investigation.⁵¹ It is necessary to have computed infrared intensities in order to identify the Al_2H_4 isomer formed here (Table 2).

The important Al_2H_6 molecule has attracted considerable theoretical attention, and these calculations reveal a stable molecule of D_{2h} symmetry and frequencies in accord with this structure.^{7–13} Table 3 compares the infrared active modes computed at SCF, CCSD, B3LYP, and BPW91 levels of theory and shows that the calculated frequencies decrease in this order. Figure 10 illustrates the B3LYP structures for Al_2H_2 , Al_2H_4 , and Al_2H_6 , which are in agreement with previous reports.^{7–13,23,50,51} These structures are useful to picture the vibrational modes. Finally,

(50) Stephens, J. C.; Bolton, E. E.; Schaefer, H. F., III; Andrews, L. *J. Chem. Phys.* **1997**, *107*, 119.

(51) Lammertsma, K.; Güner, O. F.; Drewes, R. M.; Reed, A. E.; Schleyer, P. v. R. *Inorg. Chem.* **1989**, *28*, 313.

Table 2. Calculated (B3LYP/6-311++G**) Structures and Frequencies for Aluminum Hydride and AlH₂ Molecules

molecule	length (Å); angle (deg)	frequencies, cm ⁻¹ (intensities, km/mol)
AlH (¹ Σ ⁺)	1.666	1642.2 (732)
AlH ₂ (² A ₁)	1.603; 118.1	1861.9 (b ₂ , 346), 1817.0 (a ₁ , 91), 768.9 (a ₁ , 278)
(C _{2v})		
AlH ₂ ⁺ (¹ Σ _g ⁺) ^a	1.551	2133.5 (σ _u , 0.4), 2034.9 (σ _g , 0), 567.5 (π _u , 130 × 2)
(D _{∞h})		
AlH ₂ ⁻ (¹ A ₁) ^b	1.699; 94.6	1474.4 (a ₁ , 1473), 1466.0 (b ₂ , 1466.0), 808.7 (a ₁ , 383)
(C _{2v})		
AlH ₃ (¹ A ₁) ^c	1.584	1948.7 (e, 272 × 2), 1939.1 (a ₁ , 0), 799.4 (e, 233 × 2), 713.1 (a ₂ ^{''} , 380)
(D _{3h})		
AlH ₃ ⁻ (² A ₁) ^c	1.632; 112.7	1711 (a ₁ , 193), 1698 (e, 677 × 2), 761 (e, 222 × 2), 581 (a ₁ , 319)
(C _{3v})		
AlH ₄ ⁻ (¹ A ₁) ^d	1.644	1735.4 (a ₁ , 0), 1648.5 (t ₂ , 713 × 3), 783.2 (t ₂ , 535 × 3), 763.0 (e, 0 × 2)
(T _d)		
Al ₂ (³ Π _u)	2.762	254 (0)
(D _{∞h})		
Al ₂ H ₂ (¹ A _g)	1.831; 2.976	1359 (a _g , 0), 1187 (b _{1u} , 2064), 1070 (b _{3g} , 0), 966 (b _{2u} , 118), 315 (a _g , 0), 234 (b _{3u} , 157)
(D _{2h})		
HAi(H) ₃ Al (¹ A ₁) ^e	1.578, 1.676, 1.976; 128.0, 86.0, 70.7	1953 (a ₁ , 340), 1694 (a ₁ , 75), 1574 (e, 43 × 2), 936 (a ₁ , 851), 895 (e, 46 × 2), 821 (e, 323 × 2), 411 (a ₁ , 72), 384 (e, 0 × 2)
(C _{3v})		
H ₂ Al(H) ₂ Al (¹ A ₁)	1.585, 1.715, 1.864; 125.5, 81.7, 74.0	1934 (b ₁ , 24), 1921 (a ₁ , 127), 1579 (a ₁ , 461), 1357 (b ₂ , 3), 1198 (a ₁ , 1065), 1085 (b ₂ , 395), 820 (b ₁ , 132), 730 (a ₁ , 341), 672 (a ₂ , 0), 513 (b ₂ , 29), 332 (a ₁ , 40), 127 (b ₁ , 19)
(C _{2v})		
H ₂ AlAlH ₂ (¹ A ₁)	1.594, 2.592; 115.9	1901 (a ₁ , 0), 1899 (e, 272 × 2), 1880 (b ₂ , 409), 819 (a ₁ , 0), 758 (b ₂ , 719), 549 (e, 75 × 2), 340 (a ₁ , 0), 306 (e, 73 × 2), 149 (b ₁ , 0)
(D _{2d})		

^a AlH₂⁺ is 166 kcal/mol higher energy than AlH₂. ^b AlH₂⁻ is 25.3 kcal/mol lower energy than AlH₂. ^c AlH₃⁻ is 10.1 kcal/mol lower energy than AlH₃. ^d AlH₄⁻ is 69.9 kcal/mol lower energy than AlH₂ + H₂. ^e C_{3v} structure is global minimum: C_{2v} structure is 1.6 kcal/mol higher, and D_{2d} structure is 9.4 kcal/mol higher.

Table 3. Comparison of Calculated and Observed Infrared Active Frequencies (cm⁻¹) for Dibridged Al₂H₆

sym	mode ^a	SCF/ITZP ^b	CCSD/DZP ^c	B3LYP ^d	BPW91 ^d	observed ^e	H/D ^f
b _{1u}	8	2062 (518)	2047 (344)	1989 (419)	1934 (379)	1932 (0.069)	1.366
	9	977 (393)	954 (317)	866 (244)	808 (199)	836 (0.037)	1.376
	10	249 (18)	235 (15)	223 (13)	205 (10)		
b _{2u}	13	1350 (544)	1368 (463)	1292 (352)	1275 (291)	1268 (0.053)	1.379
	14	694 (353)	664 (328)	634 (263)	607 (230)	632 (0.039)	
b _{3u}	16	2051 (101)	2024 (88)	1966 (126)	1908 (130)	1915 (0.023)	1.364
	17	1603 (1399)	1589 (1162)	1483 (1096)	1431 (968)	1408 (0.128)	1.370
	18	766 (890)	744 (684)	712 (648)	683 (575)	702 (0.048)	1.376

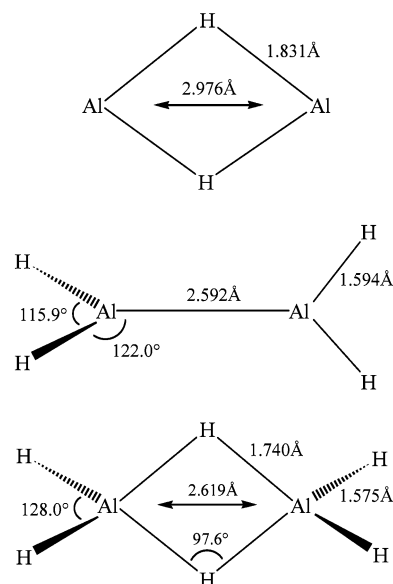
^a Symmetry (D_{2h} point group) and mode description from ref 7. ^b Reference 7; calculated intensities (km/mol) in parentheses. ^c Reference 11. ^d This work, 6-311++G** basis set. ^e In solid hydrogen, integrated intensities at maximum yield in parentheses. ^f Hydrogen/deuterium frequency ratio.

we compute Al₂H₆ in D_{3h} and D_{3d} symmetry to be two unbound AlH₃ subunits.

Discussion

The new absorptions observed here will be assigned to the Al₂H₄ and Al₂H₆ molecules on the basis of their reactions on annealing, photochemistry, behavior on deuterium substitution, and comparison to vibrational frequencies predicted by density functional calculations. This work provides the first experimental evidence for these two neutral dialane molecules.

Al₂H₄. The 1840–1780 cm⁻¹ region of our normal hydrogen matrix spectra contains five sharp peaks. The strongest band at 1821.9 cm⁻¹ is associated with the 1787.8 cm⁻¹ band on annealing and photolysis throughout these experiments: these major product bands are 15.9 and 18.2 cm⁻¹ above argon matrix AlH₂ bands^{23,25} and 6.7 and 6.9 cm⁻¹ below new neon matrix AlH₂ bands observed here. This is the relationship found for neon, hydrogen, and argon matrix absorptions of the same species.⁴⁹ The much larger argon-to-hydrogen matrix shifts for AlH₂ compared to AlH₃ (1 cm⁻¹) suggests that AlH₂ in solid hydrogen may in fact be a weak (H₂)AlH₂ complex,^{23,25} however, the 1821.9 and 1787.8 cm⁻¹ bands are sharp, and we find no evidence of an associated H–H stretching mode. In para-H₂, these bands are at 1822.0 and 1787.9 cm⁻¹. A weaker,

**Figure 10.** Structures calculated (B3LYP/6-311++G**) for the dialuminum hydrides Al₂H₂, Al₂H₄, and Al₂H₆.

sharp 770.5 cm⁻¹ band appears to be due to the bending mode of AlH₂ observed at 766.4 cm⁻¹ in solid argon.²⁵

The sharp 1838.4, 1835.8, and 1825.5 cm^{-1} bands behave as a group on annealing and photolysis. The $\lambda > 530$ and 470 nm photolysis sequence decreased AlH_2 absorptions and slightly increased the above group whereas $\lambda > 290$ nm reversed this trend and $\lambda > 240$ nm almost destroyed both band sets. The $\lambda > 380$ nm photolysis slightly decreased the above group but nearly destroyed the AlH_2 absorptions (Figure 2b). The unique nature of these sharp bands is demonstrated by their spontaneous formation on deposition in para- H_2 at 1840.9, 1838.3, and 1826.8 cm^{-1} (Figure 7).

In solid deuterium, the corresponding 1350–1290 cm^{-1} region contains four sharp peaks (Figure 4). The 1337.2 and 1293.1 cm^{-1} bands are stronger initially, and they increase on $\lambda > 290$ nm photolysis, which almost destroys the 1346.1, 1306.4 cm^{-1} set. The latter pair dominate after 9.0 K annealing (Figure 4g). The 1337.2 and 1293.1 cm^{-1} bands are 12.9 and 14.8 cm^{-1} above AlD_2 absorptions in solid argon,^{23,25} but 3.2 and 2.9 cm^{-1} below new neon matrix AlD_2 bands observed here. Thus, the 1337.2 and 1293.1 cm^{-1} bands are due to AlD_2 in solid deuterium.

The $\text{H}_2 + \text{D}_2$ experiments give several new absorptions (Figure 2d). In the Al–H region, the 1822.7, 1789.4 cm^{-1} peaks arise from AlH_2 where 0.8 and 1.6 cm^{-1} differences are due to the change from pure H_2 . The new 1807.2 cm^{-1} band is appropriate for AlHD observed 18.4 cm^{-1} lower at 1788.8 cm^{-1} in solid argon.^{23,25} New 1811.5, 1808.7 cm^{-1} bands appear to track with the 1834.7, 1832.2, 1822.9 cm^{-1} set, which exhibits different relative intensities from the analogous pure H_2 product group. In the Al–D region, new 1337.3 and 1293.3 cm^{-1} peaks are due to AlD_2 , and a new 1317.6 band is appropriate for AlHD , which is observed 18.3 cm^{-1} lower at 1299.3 cm^{-1} in solid argon.²⁵ A new 1326.3, 1325.1 cm^{-1} band appears to track with the 1346.0, 1306.8 cm^{-1} pair.

The pure HD experiment (Figures 2e and 5) behaved similarly. New bands at 1806.8 and 1315.5 cm^{-1} due to AlHD in pure HD are 0.4 and 2.1 cm^{-1} different from AlHD in the $\text{H}_2 + \text{D}_2$ sample. In addition, new absorptions are observed at 1844.5, 1840.1, 1835.2, 1831.5 cm^{-1} and at 1341.5, 1331.0 cm^{-1} .

Lammertsma et al.⁵¹ performed a detailed series of calculations on Al_2H_4 structures, and concluded that ionic C_{3v} and C_{2v} structures are slightly lower in energy than the D_{2d} H_2AlAlH_2 form. Our B3LYP calculations agree with this conclusion and provide frequencies and infrared intensities that support identification of the D_{2d} form through the 1838.4, 1835.8, 1825.5 cm^{-1} band group in solid hydrogen. The lower energy ionic C_{2v} structure is predicted to exhibit a very strong a_1 bridge stretching mode at 1198 cm^{-1} (Table 2). No absorptions appear in this region except for the very strong bridge stretching mode²³ of Al_2H_2 at 1156.1 cm^{-1} . The lowest energy $\text{HAl(H)}_3\text{Al}$ structure is predicted to have its strongest IR absorption at 936 cm^{-1} , which is antisymmetric stretching of the $\text{Al}(\mu\text{-H})_3\text{Al}$ bonds along the Al–Al axis. A weak, photosensitive 924 cm^{-1} band is likely due to this species: the deuterium counterpart is 696 cm^{-1} . The next strongest band is the degenerate H–Al bending mode, computed at 821 cm^{-1} , and the sharp 844.1 cm^{-1} band exhibits the same annealing and photolysis behavior, and is likewise assigned to the ionic $\text{HAl(H)}_3\text{Al}$ isomer of Al_2H_4 .

Two strong Al–H stretching modes are predicted at 1899 cm^{-1} (e , 544 km/mol) and 1880 cm^{-1} (b_2 , 409 km/mol) for D_{2d} symmetry Al_2H_4 (Table 2) where the former is an antisym-

metric Al–H₂ stretching mode and the latter is an out-of-phase combination of symmetric Al–H₂ stretching modes on the two AlH_2 subunits. Furthermore these modes are predicted 37 and 63 cm^{-1} above the stretching modes of AlH_2 , and the 1838.4, 1835.8 and 1825.5 cm^{-1} bands are 15 and 38 cm^{-1} higher than the AlH_2 absorptions in solid hydrogen. We also find a correspondence in the H/D isotopic frequency ratios: for AlH_2 , the H/D frequency ratios are 1.3624 and 1.3826 for the antisymmetric and symmetric modes, respectively, and for the above group 1837.1 (average)/1346.1 = 1.3648 and 1825.5/1306.4 = 1.3974. Scale factors (observed/calculated) using our hydrogen matrix and B3LYP frequencies for AlH_2 are 0.979 (b_2) and 0.984 (a_1). Similar scale factors are found for the above group: the split 1838.4, 1835.8 cm^{-1} band is assigned to the e mode and the 1825.5 cm^{-1} band to the b_2 mode of Al_2H_4 , and 0.967 (e) and 0.971 (b_2) scale factors result. All of the above evidence substantiates the present infrared identification of Al_2H_4 . The stronger e mode of Al_2D_4 is not split by the D_2 matrix. Our B3LYP calculations predict a strong AlH_2 bending mode (b_2 , out-of-phase scissors) for Al_2H_4 at 758 cm^{-1} . A broad 747 cm^{-1} band tracks with the above band group on annealing and photolysis in normal hydrogen and is assigned to the b_2 bending mode of Al_2H_4 . In para- H_2 this band is sharp at 747.8 cm^{-1} . Finally, the unique observation of these bands on deposition of thermal Al atoms with para- H_2 at 2.4 K points to a spontaneous reaction of Al_2 (see the Reaction Mechanisms section).

The mixed isotopic experiments provide further support for the identification of Al_2H_4 . Our B3LYP calculation for $\text{AlH}_2\text{-AlD}_2$ predicts two strong absorptions coincident with e modes of the pure isotopic species plus strong bands just 9 and 25 cm^{-1} lower in the Al–H and Al–D stretching regions, respectively. The new bands at 1811.5, 1808.7 cm^{-1} and 1326.3, 1325.1 cm^{-1} , which are 22 and 20 cm^{-1} lower than the corresponding bands for the pure isotopic species, are assigned to AlH_2AlD_2 . Our calculation for AlHDAIHD predicts four new observable bands in these regions, and new bands at 1844.5, 1835.2, 1341.5, and 1331.0 cm^{-1} in pure HD are appropriate for the AlHDAIHD isotopic molecule.

Although there is extensive synthetic chemistry for substituted dialane (4) compounds,⁵² this is, we believe, the first experimental evidence for dialane (4) itself, Al_2H_4 .

Al_2H_6 . The seven band DA set has straightforward chemistry. The strongest three bands at 1932.3, 1408.1, and 1268.2 cm^{-1} are detected on laser-ablated Al deposition with normal hydrogen (absorbance 0.001). These bands double on annealing to 6.0 K and double again on $\lambda > 290$ nm photolysis while AlH is reduced 90%, AlH_3 increases 4-fold, and weaker DA bands join at 1915.1, 835.6, 702.4, and 631.9 cm^{-1} . Subsequent $\lambda > 240$ nm photolysis increases the DA bands 4-fold in concert and the AlH_3 bands 2-fold, while the next 6.5 K annealing increases DA bands by 25% at the expense of AlH_3 , and a final $\lambda > 240$ nm photolysis increases DA bands by 50% and AlH_3 by 5% (Figure 1). Thus, AlH_3 is produced on photoexcitation of AlH with excess hydrogen,^{23–25} and DA is formed on ultraviolet photolysis along with AlH_3 and on annealing from diffusion and reaction of AlH_3 . The seven DA bands then must be considered for assignment to dialane, Al_2H_6 . These bands are produced in much greater yield in the softer hydrogen and

(52) Uhl, W. *Coord. Chem. Rev.* **1997**, 163, 1.

neon matrixes, which allow more diffusion, than the more rigid argon matrix. Finally, the highest frequency five of these bands are observed in para-H₂ at 1933.5, 1918.6, 1406.1, 1264.3, and 835.2 cm⁻¹ after ultraviolet photolysis.

Similar experiments were done with pure normal-D₂ and with H₂+D₂ mixtures. The perdeuterio counterparts for AlD₂, AlD₃, and all but the weakest DA band are listed in Table 1. The H/D frequency ratios ranging from 1.379 to 1.364 (Table 3) are characteristic of Al–H/Al–D vibrational modes. New information obtained from H₂ + D₂ mixtures includes new absorptions at 1925.5, 1411.7 cm⁻¹ and at 1036.6 cm⁻¹ in addition to stronger AlH₂D, AlHD₂, and AlHD absorptions.^{23–26} The new 1925.5 cm⁻¹ band between pure H₂ product bands at 1932.3 and 1915.1 cm⁻¹ (Figure 2d) and the new 1411.7 cm⁻¹ band between pure D₂ product bands at 1414.9 and 1402.9 cm⁻¹ indicate that the pure matrix bands are antisymmetric and symmetric AlH₂(AlD₂) stretching modes, and their position above AlH₂ points to a terminal AlH₂ subunit. Thus, the intermediate bands are uncoupled Al–H and Al–D stretching modes in a terminal AlHD group. In fact the H/D frequency ratios for the antisymmetric Al–H stretching modes of AlH₂ (b₂), AlH₃ (e), and Al₂H₆ (b_{1u}) exhibit almost the same H/D ratios (1.362–1.366). The 1036.6 cm⁻¹ absorption is slightly higher than 1028.5 cm⁻¹ pure deuterium counterpart, and this is consistent with an Al–(D)₂–Al bridging subunit coupled to Al–H motions. The pure HD experiment likewise produced AlH₂D, AlHD₂ and AlHD plus sharp new absorptions at 1926.5, 1922.6, 1919.4, 1915.7 cm⁻¹ (Figure 2f) and at 1416.8, 1415.0, 1412.9, 1406.4 cm⁻¹. These bands are clearly due to terminal Al–H and Al–D vibrations in mixed isotopic Al₂H_xD_y (x + y = 6) molecules. Unfortunately, the strongest Al(HD)Al bridge mode is predicted to fall under the strong AlHD₂ absorption.

Table 2 compares previous SCF and CCSD calculated frequencies^{7,11} with the present B3LYP and BPW91 harmonic predictions for Al₂H₆, which are expected to approach the experimental anharmonic values.⁵³ Notice that the BPW91-computed Al–H stretching frequencies are closer to the observed values, but the bending frequencies are below the observed values. Liang et al.⁷ also performed similar SCF calculations for B₂H₆ and Ga₂H₆ and showed that the calculated frequencies for the seven strongest infrared active modes, designated 8, 9, 13, 14, 16, 17, 18 in Table 2, are respectively 6.9, 16.4, 5.5, 9.1, 6.8, 11.6, and 8.7% higher than observed values for B₂H₆ and 3.9, 14.7, 4.1, 6.5, 5.0, 10.5, and 8.6% higher than observed for Ga₂H₆. Their calculated frequencies for Al₂H₆ are likewise 6.7, 19.3, 6.5, 9.8, 7.1, 13.8, and 9.1% higher than our hydrogen matrix DA absorptions. The correlation in these % deviations between calculated and observed M₂H₆ frequencies points to the identification of DA as dialane Al₂H₆. The 1932 and 1915 cm⁻¹ absorptions are antisymmetric b_{1u} and b_{3u} terminal Al–H₂ stretching modes. The 1408 and 1268 cm⁻¹ bands are antisymmetric b_{2u} and b_{3u} stretching modes of the bridged Al–(μ-H)₂–Al subunit. The lower frequency 836, 632, and 702 cm⁻¹ absorptions are due to AlH₂ wag, rock, and bending motions.⁷

A comparison of calculated harmonic (B3LYP) and observed anharmonic (hydrogen matrix) terminal Al–H stretching frequencies (Tables 1–3) shows that calculated exceed observed values by 40, 29 cm⁻¹ for AlH₂, 65 cm⁻¹ for AlH₃, 62, 54 cm⁻¹

for Al₂H₄, and 57, 51 cm⁻¹ for Al₂H₆. Part of this discrepancy is due to anharmonicity. The general agreement in these calculated-observed differences underscores the predictive power of quantum chemical calculations and further supports our preparation and identification of Al₂H₆.

Another means of comparison is the scale factor (observed/calculated frequencies). For our B3LYP calculation, scale factors are 0.971 and 0.974 for the terminal Al–H₂ stretching modes, 0.949 and 0.981 for the bridge Al–(H)₂–Al stretching motions, and 0.965, 0.989, and 0.997 for the low-frequency vibrations. Our scale factor for the e stretching mode of AlH₃ is 0.967. These typical scale factors for the B3LYP functional⁵³ further substantiate our identification of dialane from the matrix infrared spectrum. Note that scale factors differ for different vibrational modes: the potential functions will require anharmonic refinement for better agreement. Confidence in this identification of dialane is built on excellent agreement between observed and calculated frequencies for *seven* fundamental vibrations in three different spectral regions.

Hydrogen–argon matrix shifts observed for the strongest DA bands (Table 1) are slightly larger than those found for AlH₂, but the hydrogen–neon matrix shifts are smaller. Very weak argon matrix DA bands were detected in our earlier argon matrix investigations using high H₂ concentrations.

Additional agreement is found in the calculated and observed infrared intensities. The strongest band in the infrared spectrum, by about a factor of 2, is the antisymmetric b_{3u} Al–(μ-H)₂–Al bridge-bond stretching mode parallel to the Al–Al axis. This 1408 cm⁻¹ band in our spectrum is broader than the 1268 cm⁻¹ absorption, which is the antisymmetric b_{2u} Al–(μ-H)₂–Al bridge-bond stretching mode perpendicular to the Al–Al axis. However, the integrated experimental band intensities (Table 2) are in qualitative agreement with the predictions of theory. The terminal Al–H₂ b_{1u} and b_{3u} stretching modes are split by interaction with the hydrogen matrix. The higher frequency b_{1u} mode is predicted (B3LYP) to be 3-fold stronger, and the observed relative b_{1u} and b_{3u} mode intensities match nicely (Figure 2c).

Weaker 1362.8 and 1227.8 cm⁻¹ bands appear along with DA on λ > 380, 290 nm photolysis but decrease when DA increases markedly on λ > 240 nm irradiation (Figure 1). These bands reappear on 6.5 K annealing while DA slightly increases. The proximity to strong DA bands at 1408.1 and 1268.2 cm⁻¹ suggests that a perturbed or aggregated DA species is also formed in the hydrogen matrix. Finally, annealing produces a satellite band 8 cm⁻¹ lower than the strong e fundamental of AlD₃. Since we compute D_{3d} and D_{3h} structures to be unbound (AlH₃)₂, this satellite is probably due to (AlD₃)₂.

Alkyl substituents stabilize aluminum hydrides,⁵⁴ and the stable compound (CH₃)₂Al(μ-H)₂Al(CH₃)₂ has the same dibridged Al(μ-H)₂Al subunit as Al₂H₆.⁵⁵ Recent B3LYP calculations of the Al–H–Al bridge bond length find 1.76 Å, which is almost the same as the present 1.74 Å value for Al₂H₆, and association enthalpies computed for (CH₃)₂AlH are only 2 kcal/mol less than for AlH₃.⁵⁶ Hence, these aluminum hydride compounds have similar bridge bonding. Furthermore, calculated (B3LYP) frequencies (1442, 1245 cm⁻¹)⁵⁶ and vapor-phase absorptions

(54) Schulz, S. *Coord. Chem. Rev.* **2001**, 215, 1.

(55) Almennigen, A.; Anderson, G. A.; Forgaard, F. R.; Haaland, A. *Acta Chem. Scand.* **1972**, 26, 2315.

(56) Willis, B. G.; Jensen, K. F. *J. Phys. Chem. A* **1998**, 102, 2613.

(53) Scott, A. P.; Radom, L. *J. Phys. Chem.* **1996**, 100, 16502.

(1368, 1215 cm^{-1})⁵⁷ observed for the $\text{Al}(\text{H})_2\text{Al}$ bridge stretching modes are in excellent agreement for the $(\text{CH}_3)_2\text{AlH}$ dimer, $(\text{CH}_3)_2\text{Al}(\mu\text{-H})_2\text{Al}(\text{CH}_3)_2$, and these diagnostic frequencies are only slightly lower than our corresponding B3LYP (1483, 1292 cm^{-1}) and observed (1408, 1268 cm^{-1}) values for $\text{H}_2\text{Al}(\mu\text{-H})_2\text{AlH}_2$. A more recent investigation of gaseous $[\text{Me}_2\text{AlH}]_2$ reported a 1357 cm^{-1} infrared band and a more accurate 178 pm electron diffraction measurement for the Al–H bridge bond, and corroborating MP2 calculations.⁵⁸ These comparisons of $\text{Al}(\text{H})_2\text{Al}$ bridge stretching frequencies provide further evidence for the present experimental identification of the binary hydride dialane $\text{H}_2\text{Al}(\mu\text{-H})_2\text{AlH}_2$ molecule.

A final comparison can be made with the infrared active $\text{M}(\mu\text{-H})_2\text{-M}$ bridge stretching modes for the three M_2H_6 molecules characterized to date, $\text{M} = \text{B}, \text{Al}, \text{Ga}$. The ν_{13} (b_{1u}) modes are 1924, 1268, 1202 cm^{-1} , respectively, and the ν_{17} (b_{3u}) modes are 1615, 1408, 1273 cm^{-1} , respectively.^{15,59} The dialane frequencies are intermediate but much closer to digallane than diborane values.

We believe that the infrared spectrum of Al_2H_6 , containing seven fundamental absorption bands in terminal Al–H₂ stretching, bridge Al–(H)₂–Al stretching, and Al–H₂ bending regions, which are nicely matched by quantum chemical frequency calculations, makes a very strong case for the identification of dialane and its characterization with the diborane bridge-bonding model.⁶⁰

Al_2H_2 . The earlier argon matrix work assigned several bands to Al_2H_2 species.^{23,50} One of these absorptions is observed at 1156.1 cm^{-1} in normal and at 1155.0 cm^{-1} in para- H_2 . The former band shifts to 1102.6 cm^{-1} in pure HD and to 852.0 cm^{-1} in pure deuterium. Our B3LYP calculation predicts the extremely intense b_{1u} antisymmetric stretching mode of planar dibridged Al_2H_2 at 1187 cm^{-1} , but the corresponding b_{2u} mode is only 5% as strong, as found previously.⁵⁰ The shift to 852.0 cm^{-1} and 1.357 H/D ratio are appropriate for a bridge stretching mode. The sharp 844.1 cm^{-1} band does not track on $\lambda > 530$ nm photolysis, which destroys the 1156.1 cm^{-1} band in favor of Al_2H_6 . The 1156.1 cm^{-1} band is assigned to the most stable Al_2H_2 isomer, dibridged Al–($\mu\text{-H}$)₂–Al, which is the only form observed in solid hydrogen.

AlH_4^- , AlD_4^- , AlH_3^- , and AlD_2^- . The 1638.1 cm^{-1} absorption appears above a 1609.3 cm^{-1} photolysis product in the argon/ Al/H_2 system, which has been conclusively identified as AlH_4^- isolated in solid argon.⁴⁸ The 1638.1 cm^{-1} band increases on $\lambda > 380$, 290 nm photolysis but decreases on $\lambda > 240$ nm irradiation (Figure 1). Furthermore, the 1638.1 cm^{-1} band decreases in yield relative to the AlH_3 band with increasing laser energy. In pure deuterium the 1183.2 cm^{-1} counterpart is weak, but a 1050.0, 1043.0 cm^{-1} doublet gives way on $\lambda > 290$ nm photolysis and doubles the 1183.2 cm^{-1} absorption, but $\lambda > 240$ nm irradiation virtually destroys this feature. Pure HD gives new counterpart absorptions at 1658.1 and 1193.9 cm^{-1} for AlH_2D_2^- , which supports assignment of the 1638.1 cm^{-1} band to AlH_4^- in solid hydrogen. This is in agreement with the present and previous⁴⁸ DFT calculations for the ν_3 (t_2) fundamental of tetrahedral AlH_4^- .

The photosensitive 1050.0, 1043.0 cm^{-1} band pair in solid D_2 is extremely close to our B3LYP prediction of 1058.4 (a_1) and 1056.9 cm^{-1} (b_2) modes for AlD_2^- . Since our B3LYP calculation found 1190.2 cm^{-1} for ν_3 (t_2) of AlD_4^- , only 7.0 cm^{-1} above the observed value in solid D_2 , the 1050.0 and 1043.0 cm^{-1} bands are assigned to ν_1 (a_1) and ν_3 (b_2) of AlD_2^- . This observation means that AlD_2^- is stable in solid D_2 , but $\lambda > 290$ nm radiation initiates reaction with D_2 to form AlD_4^- . However, the corresponding AlH_2^- species was not observed in solid H_2 . This suggests that any AlH_2^- formed reacts straightaway with H_2 to form AlH_4^- , which is observed at 1638.1 cm^{-1} in solid H_2 .

Our B3LYP calculations show that AlH_3^- is a stable anion, more so than BH_3^- , which has been characterized.³⁰ The AlH_3^- anion is computed to be 10.1 kcal/mol more stable than AlH_3 , to be pyramidal (112.7° H–Al–H angle), and to have a strong ν_3 (e) mode at 1698 cm^{-1} . A sharp, very weak 1701.6 cm^{-1} absorption decreases on 6.2 K annealing and disappears on $\lambda > 380$ nm photolysis: this band could be due to AlH_3^- , but we cannot be certain without more evidence.

Solid $(\text{AlH}_3)_n$. When the hydrogen matrix samples are annealed to 6.8 K, H_2 evaporates, molecular aluminum hydrides diffuse, aggregate and their absorptions decrease, and broad absorptions appear at 1720 ± 20 and 720 ± 20 cm^{-1} (Figure 3a–c). These broad bands remain on the CsI window with decreasing absorbance until room temperature is reached. The deuterium matrix samples evaporate D_2 at about 10 K and aluminum deuterides produce a broad 1260 ± 20 cm^{-1} absorption (Figure 3d,e), which remains on the CsI window. The frequency ratio $1720/1260 = 1.365$ demonstrates that these bands are due to Al–H/Al–D vibrations. The aluminum/ H_2 / D_2 samples produce similar broad bands after evaporation of the matrix that are shifted slightly to 1740 ± 20 , 1280 ± 20 , and 710 ± 20 cm^{-1} (Figure 3f).

The spectrum of pure solid $(\text{AlH}_3)_n$ gives strong broad bands at 1760 and 680 cm^{-1} , solid $(\text{AlH}_3)_n$ in Nujol reveals a very strong, broad 1592 cm^{-1} band, and solid $(\text{AlD}_3)_n$ gives a corresponding 1163 cm^{-1} band.^{61,62} The present broad absorptions at 1720 and 1260 cm^{-1} are therefore due to solid $(\text{AlH}_3)_n$ and $(\text{AlD}_3)_n$ on the salt window. Since the Al–H bond is polar,¹⁶ the solid $(\text{AlH}_3)_n$ network⁵ may align and bind electrostatically to the ionic CsI lattice surface. The 100 cm^{-1} redshift in Nujol is due to interaction with this host medium.

Our broad 720 cm^{-1} absorption corresponds to the 680 cm^{-1} solid band.⁶¹ These bands are higher than our 632 cm^{-1} Al_2H_6 absorption, which probably involves bending of the Al–H–Al bridge bonds. A very weak 520 ± 20 cm^{-1} absorption on our cold window (Figure 3e) may be the deuterium counterpart of the 508 cm^{-1} Nujol band.

The crystal structure for solid $(\text{AlH}_3)_n$ shows six-coordinate aluminum with equivalent hydrogen atoms in bridge-bonding arrangements between aluminum atoms.⁵ The average Al–H distance is 1.72 Å. It is interesting to note that the solid Al–H distance is intermediate between the 1.74 Å bridge and 1.58 Å terminal Al–H distances calculated here for Al_2H_6 and that the solid frequency of 1720 cm^{-1} is likewise intermediate between

(57) Grady, A. S.; Puntambekar, S. G.; Russell, D. K. *Spectrochim. Acta* **1991**, 47A, 47.

(58) Downs, A. J. et al. *Organometallics* **2000**, 19, 527.

(59) Duncan, J. L. J. *Mol. Spectrosc.* **1985**, 113, 63.

(60) Price, W. C. *J. Chem. Phys.* **1948**, 16, 894.

(61) Matzek, W. E.; Musinski, D. F. U.S. Patent 3,883,644, 1975; *Chem. Abstr.* **1975**, 83, 45418.

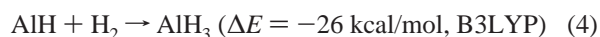
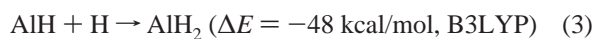
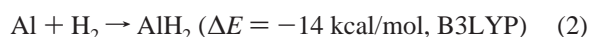
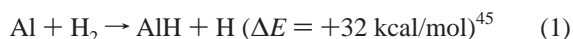
(62) Roszinski, W.; Dantel, R.; Zeil, W. Z. *Physik. Chem. (Frankfurt)* **1963**, 36, 26.

the terminal (1932, 1915 cm^{-1}) and bridged (1408, 1268 cm^{-1}) Al_2H_6 values observed here.

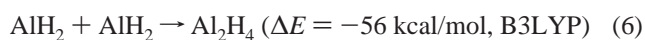
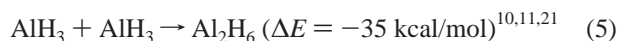
Evaporation of the H_2 , D_2 matrix from mixed H, D-aluminum hydride samples gave similar broad bands slightly blue shifted. This shows a slight stretch-stretch interaction for Al–H–Al bonds in the solid state and suggests that the symmetric stretching modes in $(\text{AlH}_3)_n$ are higher than the observed antisymmetric stretching modes.

Finally, it is interesting to observe that these reactions take Al and H_2 to the molecular aluminum hydrides AlH_3 and Al_2H_6 , which aggregate in the end to form solid $(\text{AlH}_3)_n$ films. Thus, we have explored aluminum–hydrogen chemistry from the microscopic beginning to the macroscopic end using the matrix isolation technique.

Reaction Mechanisms. The reaction of Al and H_2 to form AlH must be activated by photolysis^{24,25,63} or by excess energy (kinetic or photon) from the ablation process.^{32,64} Even though reaction 2 to form AlH_2 is exothermic, it must also be activated by ultraviolet photolysis.^{25,65} Furthermore, the observation of AlH in solid H_2 requires a barrier for reaction 4.

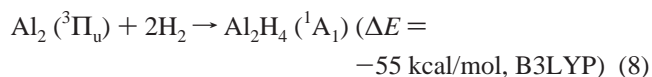
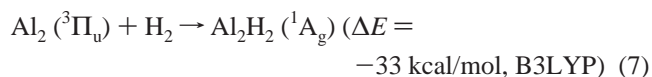


The growth of AlH_2 on annealing, Figure 1f, requires that H atoms diffuse and react with AlH, reaction 3. The production of H atoms in laser ablation/solid hydrogen experiments has been documented through the observation of HO_2 radical.⁴⁹ Photoexcitation of AlH at 3.0 eV (Figure 1c) in the presence of hydrogen leads to the formation of AlH_3 , reaction 4. Then Al_2H_6 is formed by the dimerization of AlH_3 , reaction 5. Although a small growth of Al_2H_6 absorptions is found on annealing the solid hydrogen samples, more growth is observed on $\lambda > 240 \text{ nm}$ irradiation when the AlH_3 monomer yield increases markedly. A strong satellite absorption at 1370.5 cm^{-1} on the 1378.7 cm^{-1} AlD_3 absorption is probably due to unreacted $(\text{AlD}_3)_2$ dimers. The absence of a similar satellite absorption for AlH_3 suggests a small activation energy for reaction 5 in the case of AlD_3 . The straightforward formation of Al_2H_4 (D_{2d}) involves the exothermic dimerization of AlH_2 , reaction 6. We find evidence for one of the ionic Al_2H_4 isomers.⁵¹ With laser-ablated Al atoms, Al_2H_4 is formed on sample deposition when the yield of AlH_2 is large, and Al_2H_6 is favored after ultraviolet photolysis when the yield of AlH_3 is high.

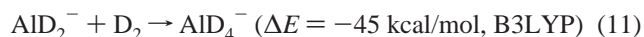
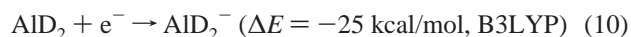
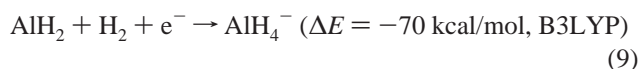


A unique synthesis of Al_2H_4 is observed from the recombination of thermal Al atoms during deposition in para- H_2 ; see

especially Figure 7a where Al_2H_4 dominates over the small amount of AlH produced during deposition by the ultraviolet spectroscopic diagnostic. Apparently the exothermic ($-30.0 \pm 1.4 \text{ kcal/mol}$) dimerization of Al atoms to form $^3\Pi_u$ ground-state Al_2 ^{66,67} is sufficient to activate one or two dihydrogen molecules to form Al_2H_2 and Al_2H_4 , reactions 7 and 8. This is consistent with our previous nonobservation of B_2 in the para- H_2 matrixes produced under conditions which yielded B_2 in rare gas matrixes.³¹ Hence, variable amounts of Al_2H_2 and Al_2H_4 are observed from these “recombination” reactions on thermal Al deposition with para- H_2 . Even though the Al_2 reaction with 3H_2 is even more exothermic (-87 kcal/mol , B3LYP), inserting $(\mu\text{-H})_2$ into the Al–Al bond in Al_2H_4 must require substantial activation energy. However, dibridged Al– $(\mu\text{-H})_2$ –Al can be activated by $\lambda > 530 \text{ nm}$ photolysis to form Al_2H_6 in solid hydrogen. Furthermore, Al_2 is similar to Ga_2 , which reacts spontaneously with H_2 in solid argon to form dibridged Ga $(\mu\text{-H})_2$ –Ga.⁶⁸ Finally, similar laser-ablated Ga experiments with pure H_2 give the analogous products including Ga_2H_2 , Ga_2H_4 , Ga_2H_6 , and GaH_2^- , which will be described in a later publication.⁶⁹



The stable AlH_4^- anion is formed by capture of electrons from the ablation process. We note that no AlH_4^- counterpart is observed with thermal Al atoms in para- H_2 . The electron affinity of AlD_2 is estimated as 25 kcal/mol (B3LYP). In solid deuterium experiments, AlD_2^- is trapped and $\lambda > 290 \text{ nm}$ photoexcitation leads directly to AlD_4^- .



The final reaction, the formation of solid aluminum hydride, occurs on evaporation of the hydrogen matrix to allow association of molecular aluminum hydrides, which can be monitored by the loss of characteristic solid hydrogen absorptions.⁷⁰ This solid $(\text{AlH}_3)_n$ is identified by agreement of broad infrared absorption bands with spectra of the pure solid.⁶¹ Reaction 12 is estimated to be exothermic by 40 kcal per mole of AlH_3 , which contributes to the stability of the solid.¹⁶ It appears, then, that the failure to isolate pure Al_2H_6 is due to its polymerization

(63) Parnis, J. M.; Ozin, G. A. *J. Phys. Chem.* **1989**, 93, 1215.

(64) Kang, H.; Beauchamp, J. L. *J. Phys. Chem.* **1985**, 89, 3364.

(65) Knight, L. B.; Woodward, J. R.; Kirk, T. J.; Arrington, C. A. *J. Phys. Chem.* **1993**, 97, 1304.

(66) Cai, M. F.; Dzugan, T. P.; Bondybey, V. E. *Chem. Phys. Lett.* **1989**, 155, 430.

(67) Fu, Z.; Lemire, G. W.; Bishea, G. A.; Morse, M. D. *J. Chem. Phys.* **1990**, 93, 8420.

(68) Himmel, H.-J.; Manceron, L.; Downs, A. J.; Pullumbi, P. *J. Am. Chem. Soc.* **2002**, 124, 4448.

(69) Wang, X.; Andrews, L. Unpublished results (Ga in H_2).

(70) Gush, H. P.; Hare, W. F. J.; Allin, E. F.; Welsh, H. L. *Can. J. Phys.* **1960**, 38, 176.

into the more stable network solid, which is observed at the end of these hydrogen matrix experiments.



The successful synthesis and characterization of Al_2H_6 is made possible by special chemical and physical properties of the pure hydrogen matrix. The “high” hydrogen concentration ensures the formation of a large yield of AlH_3 and the soft nature of solid hydrogen allows diffusion and dimerization of AlH_3 to Al_2H_6 . When the temperature of the solid hydrogen sample approaches 7 K, H_2 evaporates, the diffusion and reaction of trapped aluminum hydride molecules is rapid and solid $(\text{AlH}_3)_n$ is formed.

Conclusions

The reaction of laser-ablated Al atoms and normal- H_2 during co-deposition at 3.5 K forms AlH , AlH_2 , AlH_3 , and Al_2H_2 based on infrared spectra, and the results of isotopic substitution (D_2 , $\text{H}_2 + \text{D}_2$ mixtures, HD). Four new bands are assigned to Al_2H_4 with the D_{2d} structure. Ultraviolet photolysis markedly increases the yield of AlH_3 and seven new absorptions for Al_2H_6 in the infrared spectrum of the solid hydrogen sample. Complementary results are found using thermal Al atoms and para- H_2 . These seven vibrational frequencies are accurately predicted by quantum chemical calculations for dibridged Al_2H_6 , which is isostructural with diborane.

Annealing these samples to remove the H_2 matrix decreases the sharp AlH_3 and Al_2H_6 absorptions and produces broad 1720 ± 20 and $720 \pm 20 \text{ cm}^{-1}$ bands, which are due to solid $(\text{AlH}_3)_n$ on the CsI window. In fact laser-ablation of Al into pure hydrogen appears to be an effective method for producing an aluminum hydride film. This contrasts the case of B_2H_6 , which forms a molecular solid and gives broad bands near isolated molecule values³⁰ and the case of Ga_2H_6 , which forms an oligomer¹⁶ and gives similar film spectra^{15,69} after the hydrogen matrix evaporates.

Small matrix shifts are observed between normal hydrogen (3/4 ortho- H_2 , 1/4 para- H_2)⁷¹ and para- H_2 . The formation of Al_2H_4 during thermal Al atom deposition in para- H_2 from the exothermic combination of Al atoms assists in the matrix identification of this novel molecule.

Although many volatile binary boron hydride compounds are known, binary aluminum hydride chemistry is limited to the polymeric $(\text{AlH}_3)_n$ solid. Our experimental characterization of the dibridged Al_2H_6 molecule provides an important link between the chemistries of boron and aluminum.

Acknowledgment. We thank G. V. Chertihin and P. F. Souter for work on earlier argon matrix experiments and NSF Grant No. CHE00-78836 for financial support.

JA0353560

(71) Silvera, I. F. *Rev. Mod. Phys.* **1980**, 52, 393.